Materials Research. 2019; 22(suppl.1): e20190247
DOI: http://dx.doi.org/10.1590/1980-5373-MR-2019-0247

Effect of Nitrogen Addition to Shielding Gas on Cooling Rates and in the Microstructure of Thin Sheets of Duplex Stainless Steel Welded by Pulsed Gas Tungsten Arc Welding Process

Evandro Giuseppe Betini[a]*, Maurilio Pereira Gomes[a], Cristiano Stefano Mucsi[a], Marcos Tadeu D'Azeredo Orlando[b], Temístocles de Sousa Luz[b], Marie-Noëlle Avettand-Fénoël[c], Jesualdo Luiz Rossi[a]

[a]Instituto de Pesquisas Energéticas e Nucleares (IPEN), São Paulo, SP, Brasil
[b]Departamento de Engenharia Mecânica, Universidade Federal do Espiríto Santo, Vitória, ES, Brasil
[c]Unité Matériaux et Transformations, Université de Lille, Cité Scientifique, Villeneuve d'Ascq, França

Received: March 16, 2019; Revised: June 03, 2019; Accepted: June 24, 2019

The effect of the nitrogen content in the shielding gas and its effect on temperature distributions at the welded zone of thin sheets of duplex stainless steel have been evaluated. The duplex stainless steels have many features due to unique microstructural combination of austenite and ferrite grains. The phase balance can be easily shifted depending on the welding parameters. Two sheets were welded using pure argon and pure argon plus 2% of nitrogen as shielding gas. The thermal profile had shown that N_2-supplemented shielding gas lead to higher peaks of temperature using similar welding parameters. Microstructural examination showed that the austenite phase in the weld increased with the presence of nitrogen in the shielding gas. The added nitrogen promoted primary austenite formation and slightly increases the microhardness at the solidified zone. Microhardness mapping and metallographic imaging presented information about microstructures, confirming the formation of secondary phases during thermal cycle in the temperature range 850 °C and 950 °C. Control of ferrite amounts in the welds is essential mainly to improve mechanical properties and corrosion resistance of welding zones.

Keywords: *duplex stainless steel, cooling rates, nitrogen, GTAW, thermal cycle, microhardness.*

1. Introduction

Duplex stainless steels (DSS) have basically a microstructure consisting of austenite and ferrite. In general, DSS has around 50% of each phase in the base material but typically a variation of 35 to 60% in ferrite content results in acceptable properties[1,2].

The main commercial factor pushing the advance, the development and use of duplex stainless alloys was the increase of activity in the offshore oil industry which demanded a stainless steel material to handle aggressive environments and new steel production techniques[2]. The new technique using addition of nitrogen and lowering of carbon content made it possible to produce much cleaner steels improving high temperature stability as shown by duplex structure[1-5]. Thus, the DSS alloys have become a suitable alternative to austenitic stainless steels due to their special combination of good mechanical properties and corrosion resistance and lower costs[1,2,6]. The nuclear industry, especially requests alloys with high thermal stability in pipes for power generation systems and safe transportation equipment's for radioactive material[7-9]. DSS also presents satisfactory weldability, however it is possible to occur the formation of excessive ferrite, nitrides and intermetallic phases in the solidifying zone (SZ) and in the heat affected zone (HAZ)[1,2,10]. These formations of deleterious phases need to be avoided and a balanced ferrite / austenite microstructure must be maintained[11].

The GTAW (gas tungsten arc welding) processes are generally preferred because they produce very high-quality welds[2,3,12]. In many cases distortion is the major problem in welding of thin sections. However, the distortion is controlled in pulsed and magnetic arc oscillation GTAW process[12]. Weld root quality of stainless-steel pipe and tubes can be ensured by using an inert purging gas[3,5,11]. The pure Ar is the most commonly used purging gas in GTA welding of several grades of steels[7,11]. However, 2% nitrogen is recommended in pure argon mixture for shielding gas and optimizing the phase balance, impact toughness and corrosion resistance of DSS[13]. Taking all aspects into account, Ar + 2%N_2 is the preferred shielding gas for welding duplex and super duplex with the GTAW process[6,9].

Several authors have been mentioning the important role of N_2 in the microstructure evolution by being the strongest austenite forming alloying element[6,9,10,13-17]. Moreover, N_2 is an economical and efficient substitute for nickel[10,17]. Generally, DSS has a low bulk nitrogen content standardized in the range 0.15% - 0.35%. Moreno et al.[17] determined using electron probe microanalysis (EPMA) technique an average content of N_2 in the range 0.045% - 0.070%wt in ferrite and 0.520% - 0.770%wt in austenite for five different DSS alloys. The addition of C and N_2 strengthens both ferrite and austenite by dissolving at interstitial sites in the solid solution[2,16,17,18].

*e-mail: evandrobetini@gmail.com

During welding process, the austenite dissolves while being heated, it is followed by grain growth in the delta ferrite region, and finally restoring to the austenitic phase during cooling[19,20]. However, the loss of nitrogen and a decrease of austenite content during GTAW welding would lead to toughness reduction[10,17]. Hosseini et al.[10] monitored economical content and microstructure for each weld pass in super duplex stainless steel, by using wavelength dispersive X-ray spectrometry; It was observed that after four passes a loss of nitrogen from 0.28% in the base metal - BM to 0.17% (in mass) for low heat input. Karlsson et al.[21] using low heat input autogenously laser welding on 2507 SDSS observed highly ferritic microstructures with nitride precipitates due to nitrogen loss at high cooling rates. During the thermal cycle, the alloy is heated to a very high temperature above 1350 °C for a short time, held for a few seconds and subsequently cooled to room temperature[21,22]. Later on, in the cooling stage, the austenite re-precipitates around ferrite grain boundaries[23]. In this way, adjustment of a low cooling rate and proportion of N_2 allows adequate austenite formation, but not too low cooling rate in order to avoid precipitation of intermetallic phases[18,22-24]. Westin[24] reported that high ferrite contents resulted in Cr-rich nitrides formation in HAZ and SZ due to large ferrite grain supersaturated in nitrogen. If the gas protection is insufficient during welding or if the nitrogen is added to the shielding gas, the formation of chromium nitrides caused by an uptake of nitrogen from the atmosphere may occur[23].

Nitrogen is added to argon shielding gas in duplex stainless-steel welds to preserve weld metal nitrogen levels[15,16]. According to Zhang et al.[15], there are two ways to compensate for the nitrogen loss during welding: one is directly adding the nitrogen to the BM and filler wires in the originally producing supplies[13,17,23] or a proper proportion of nitrogen gas is added into shielding gas and backing gas during welding[11,14,16,24-28].

The main goal in the present work was to assess the effects of the nature of the nitrogen amount in the shielding gas (2% N_2 in Ar) on cooling rates, microstructural properties, microhardness and grain size of 1.8 mm thickness sheets of UNS S32304 duplex stainless-steel autogenously welded by pulsed GTAW process. The amounts of phases were evaluated by microstructural image phase analysis and electron probe microanalysis (EPMA) technique was used to measure the N_2 contents in transversal profile of welds.

2. Materials and Methods

The specimens were obtained with dimensions of 72 x 72 x 1.8 mm^3. Table 1 shows the chemical composition of used UNS S32304 duplex stainless steel. The alloy's chemical composition was certified by the commercial supplier Aperam South America S/A.

The microstructure of the ferrite and austenite was observed by optical microscopy (OM). The specimens for microstructure investigation were ground successively from P300 to P2000 grit emery paper and polished using diamond pastes of 6 µm, 3 µm and 1µm. With the purpose of characterization of various types of austenites in the welding zones, the as-polished specimens were etched in Behara I solution for 15-20 s. The optical microstructures of the SZ and HAZ were observed by means of the Image J® software with bright light micrographs according to ASTM E562[29] standard to determine the phases ratios. The free application 3D Builder® was used to better illustrate dual phase proportion in base metal and solidified zone.

Thin samples were clamped in a welding table in order to reproduce the conventional set welding process. The DSS sheets were welded using GTAW process with pulsed current and direct polarities were used with automatic drive systems. The batch of samples was welded using two commercial kinds of pure argon and a mixture of argon and 2% of nitrogen shielding gas. The gas flow rate in both cases was 10 $L.min^{-1}$. The schematic diagram of the welding process is shown in Figure 1.

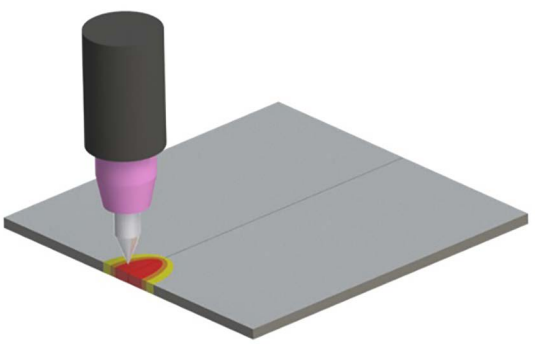

Figure 1. Schematic impression of the GTAW process on thin plates of duplex stainless steel UNS S32304.

Table 1. Chemical composition (% mass and ppm) of the duplex stainless steel UNS S32304 used in the present study.

Cr	Ni	Mo	Mn	Si	C	P	S	Ti	Cu	Co	N_{ppm}	Fe
22.210	3.521	0.255	1.402	0.250	0.016	0.023	0.001	0.004	0.417	0.091	1030	Bal.

The AWS Class EWTh-2 electrode was kept negative and was located at 2 mm with a 60° angle from the sheet, according to direct polarity process. The electrical current and voltage values were measured for each welding step. In the case of the pulsed current, the wave was maintained in balance with background time and pulse values equal to 0.9 s. Table 2, indicates the welding and thermal cycle parameters.

Regarding the parameters such as voltage (U), pulsed and background current (I_p, I_b), pulsed and background time (t_p, t_b), the welding speed (v) along with 60% arc efficiency for the pulsed GTAW welding, it was possible to calculate the welding heat input (H) per mm using equation 1[12]. The welding heat input shown in Table 2 was determined using the average voltage, current and welding speed.

$$H = \frac{60.U.(I_p.t_p + I_b.t_b)}{(t_p + t_b).v} \quad (1)$$

The thermal cycles were measured during welding by inserting thermocouples type K and S in the UNS S 32304 DSS sheet, in small drilled holes and inserting the thermocouple tip in this hole. The temperature was measured and recorded using a data acquisition system. Four thermocouples were positioned and fixed to the sample sheet's surface at different distances, along transversal and longitudinal lines of the weld bead. The thermocouples were located at 0 mm, 3 mm and 4.5 mm from the joint line.

The signals from the thermocouples were acquired by 8-channel universal data acquisition system amplifier using MX board - PT1000 for room temperature automatic conditioning. The measured total error limit at 300 K ambient temperature was ± 1 K and the temperature drift (K type) was used K/10K ratio where the uncertainty was ≤ ± 0.5.

An electron probe micro-analyzer (EPMA) was used to quantitatively evaluate the nitrogen in the welded regions. This electronic microprobe is equipped with four WDS (wavelength dispersive spectrometer) spectrometers. For the point quantifications it was used voltage acceleration of 10 kV and beam current of 100 nA.

The crystal used to detect the Kα of N was PC2. The N_2 profile was composed of EPMA-WDS point analyses distributed over a 4300 µm line for sample welded using pure Ar and a 4500 µm line for welding using Ar+2%N_2 shielding gas, crossing the base metal, heat-affected zone till center of solidified zone.

Vickers microhardness was performed for both welds using 0.5 N of load for 15 s ($HV_{0.05}$). A microhardness tester was used to determine microhardness maps on the cross sections of the welded sheets. The thickness of the sheets is 1.8 mm. In the total, five lines with 140 hardness points for 60 µm steps were performed for each sample passing through the base metal, ZAC and SZ.

3. Results and Discussion

In order to study thermal cycles, the temperature distributions were plotted for both specimens as shown in Figure 2. First, the sheet welded using pure Ar as shielding gas is shown in Figure 2a. The thermocouples TK1 and TK2 (4.5 mm away from the welding line) were placed closer to the weld bead where the peaks of temperature and cooling rate were close to 543 °C with 10.6 °C.s^{-1} and 556 °C with 12.1 °C.s^{-1}, respectively. In this region of the sheet (HAZ), the holding time were maintained between 500 °C and 600 °C for 6 s, approximately, for both TK1 and TK2 thermocouples that leads to precipitations of secondary phases as α', σ, ε and π[15,22,25]. The TK3 thermocouple presented a peak of temperature around 760 °C at 3 mm away from the center of welding line. This value is higher than that obtained in other thermocouples for the HAZ which was measured a cooling rate of 53.2 °C.s^{-1}. The welding process with high cooling rate lead to ferritization with coarse grains of ferrites in the welding zone[30].

The Figure 2b shows the thermal cycles for welding with Ar+2%N_2 as shielding gas. The thermocouples TK1 and TK2 (4.5 mm distant from the melting pool) presented peaks of temperature and cooling rates near to 759 °C - 25.2 °C.s^{-1} and 773 °C - 26.5 °C.s^{-1}, respectively. The holding time were maintained above 700 °C for 4 s which would lead to possible intermetallic phases as $M_{23}C_6$, γ_2, χ and σ[22,30]. For TK1 and TK2 also were subjected to holding time above 500 °C for 15 s approximately that would lead to higher precipitation of secondary phases such as α', ε and π[15,22,30].

Table 2. Welding parameters used for the pulsed GTAW process.

Sample	#6	#7
Shielding gas (10 L.min^{-1})	Pure Ar	Ar+2%N_2
Voltage (V)	11	11
Pulse current - I_p (A)	150	140
Background current - I_b (A)	80	70
Pulse time - t_p (ms)	0.9	0.9
Background time - t_b (ms)	0.9	0.9
Welding speed (cm.min^{-1})	35	35
Arc efficiency (%)	60	60
Heat input (kJ.mm^{-1})	0.20	0.17

Through the TK3 thermocouples it is shown a temperature peak and cooling rate around 947 °C and 27.5 °C.s^{-1} at 3 mm from the center of the solidified zone. Through the thermal cycle it is also possible to suggest that the beneficial effect of the addition of 2% N_2 on the stabilization of the temperature distribution during cooling process. This stabilization can be seen from 56 s at time on the graph shown in Figure 2b, and it can be observed that all curves are dropping at the same slope. This curve behavior could not be observed for the sample welded using pure Ar (Figure 2a). Lin et al.[31], also showed that the peak temperature of a thermal cycle increased with increasing N_2 content as more heat is carried into shielding gas. Thus, increasing the N_2 content more heat is carried into the work piece and increases the weld metal area[32]. In addition, according to the study by Tseng and Chou[12], using pulsed GTAW process higher ratio amplitude can reduce the temperature difference between the melting zone and the unaffected base metal in welding and therefore the welding residual stress can be reduced.

The Figure 3 shows the temperatures obtained on the bottom of the center of welding zone (0 mm) and HAZ (3 mm and 4.5 mm) during passage of the welding. In these points it was obtained values in the order of 1173 °C for welding with pure Ar and 1221 °C for welding with Ar + 2% N_2, which suggests an influence of the shielding gas on the temperature distribution of welding. In addition, all welding points measured with the mixture of Ar + 2% N_2 presented higher temperature than welding with pure Ar.

Figure 4 shows an optical micrograph of the microstructure that consisted of austenite and ferrite for the as received material. The ferrite phase is shown as dark, while the light region is austenite phase (see Figure 4a). In the continuous ferrite matrix is embedded island-like austenite phase without apparent secondary phase precipitation. Both grains are elongated along the rolling direction. Figure 4b shows the quantitative evaluation of the content of both ferrite and austenite phases. Based on microstructural investigations and using image analyzer software the amounts of phases in different zones of the joints were estimated. Up to five OM images were collected for each zone (SZ, HAZ and BM) and then were processed.

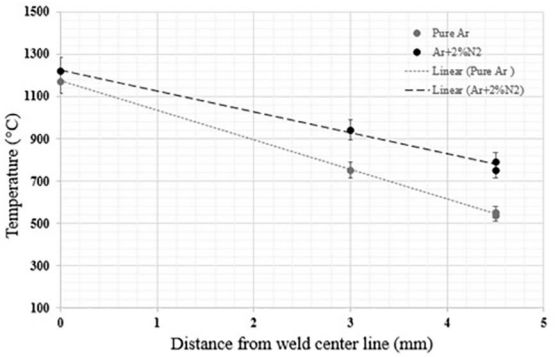

Figure 3. Peaks of temperature for thermal cycles of welding.

In order to detail the modifications in the biphasic microstructures and content variations of phases due to the welding conditions, optical micrographs were obtained, and the separation of the ferrite and austenite phases was attained with image editing effect.

Micrographs for both samples are shown in Figure 4 using the modified Behara I reagent to reveal the etched microstructure. The chemical etching resulted in a blue coloration for ferrite and a yellow coloration for austenite as reported in the literature[15,33,34].

The Figure 4 b shows the micrograph of the solidified zone for welded sheet using pure Ar as shielding gas. The Behara I reagent also resulted in dual effect of dark colors (blue) for ferrite and clear (yellow) for the austenite microstructure.

In this way, through the chemical etching it was possible to observe the ferrite morphology separately from the austenite as well as the austenite fraction phase resulting from the welding process with pure Ar as shielding gas. Besides that, secondary austenite was observed quite dispersed inside the ferrite coarse grains.

The microstructure of the solidified zone of the sample welded with Ar + 2% N_2 as the shielding gas using purge gas is presented Figure 4c. For the identification of ferrite and austenite phases, the same modified Behara I etching was used.

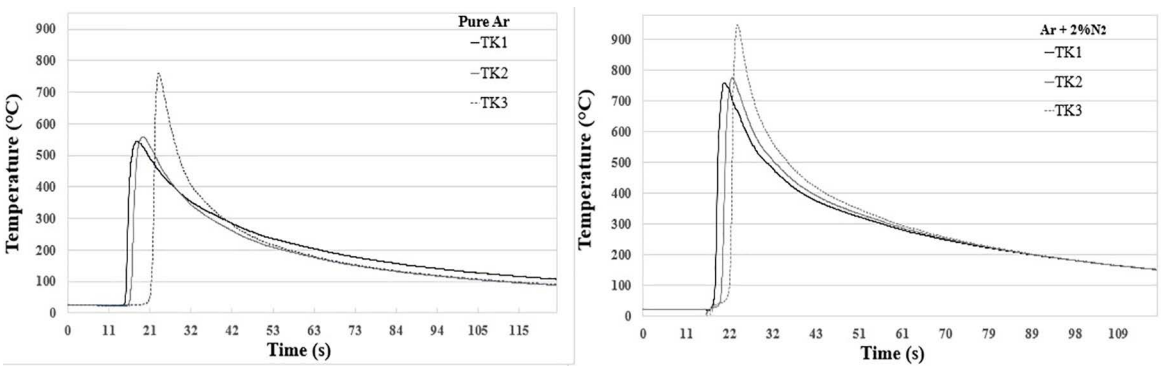

Figure 2. Distribution of temperatures for samples (a) pure Ar and (b) Ar + 2% N_2 with pure argon as purging gas. It shows the temperature variation measured with each thermocouple for the UNS 32304 duplex stainless steel, 1.8 mm long stripe, while being welded.

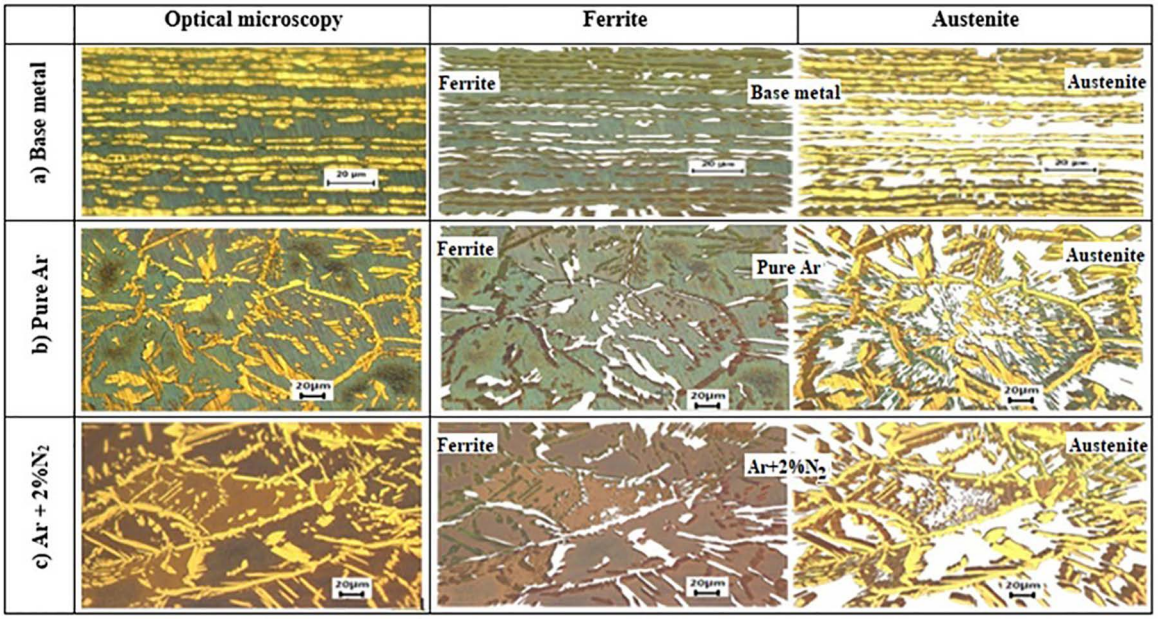

Figure 4. Microstructure of the transversal profiles of the both samples welded with a) pure Ar and b) Ar+2%N_2 as shielding gas.

For ferrite resulting from the nitrogen addition in shielding gas, it is shown as a dark (brown) color and the voids that are occupied by the austenite. For austenite shown in bright light (yellow) color, this phase is more evident in the regions at the grain boundary of ferrite and less dispersed than the sample welded with pure Ar (see Figure 4b). Thus, the separation of the phases as presented in Figure 4, shows the relationship with the changes of the austenite fractions as described in the diagram showed in Figure 5.

Figure 5 shows the evolution of the austenite volumetric fraction regarding the composition of the shielding gas in the SZ, HAZ and BM. The percentages of austenite are significantly affected by the addition of nitrogen in the shielding gas and this leads to changes in the total austenite content after the welding process. About N_2 supplementation in the shielding gas, the increase of the austenite content in the SZ was shown: 22% to 37% and HAZ: 23% to 25.3%, which agrees with the results of Tahaei et al.[35] and Zhang et al.,[15].

The addition of N_2 in the shielding gas significantly increases the amount of austenite for the DSS and GTAW welds. Zhang et al.[15] reported that N_2 in the shielding gas mainly promotes the formation of primary austenite, suppressing Cr_2N precipitation at the root of the weld. According to Westin et al.[28], nitrogen can increase the temperature of ferrite transformation into austenite. Consequently, the higher content of nitrogen makes the alloy less sensitive to the fast cooling rates due to more efficient austenite reform and delays the ferritization[28]. As seen in the present work, the microstructural changes in DSS that occur during welding can lead to the variation of the phase balance in SZ and HAZ.

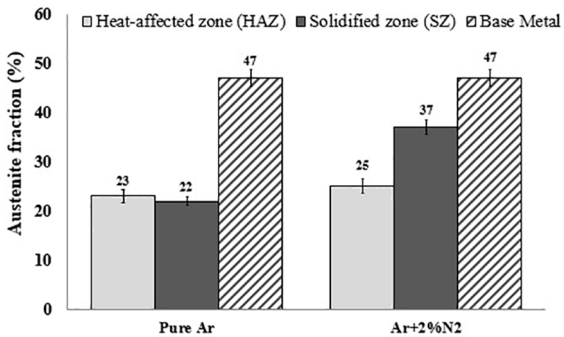

Figure 5. The effects of shielding gas composition on the austenite content of the HAZ and solidified zone in DSS.

In Figure 6, the microstructures of the UNS S32304 duplex alloy are shown in three different orthogonal directions. The first image, Figure 6a, shows the base metal in the three directions with indication of the rolling directions. No intermetallic phase was observed, both for samples as received and for the base metal.

The evolution of the microstructure of ZTA and SZ is strongly dependent on the base metal microstructure, peak temperature, residence time at high temperatures and cooling rates[13]. DSS typically have δ ferrite, primary austenite γ_1, secondary austenite γ_2, σ, χ, carbides and nitrites. For the solidified zone of DSS, the austenite phases are generally formed from ferrite in different modes: allotriomorphic austenite in the borders of ferrite grains (GBA), intragranular austenite (IGA) and austenite Widmanstätten (WA) within the grains[36].

For Figure 6b and Figure 6c, the effects of GTAW welding with 99.9% Ar as shielding gas and a mixture of Ar + 2% N_2 in three orthogonal directions are presented. The microstructure observed in both welded samples consists of large ferrite grains with intragranular austenite, grain border austenite and Widmanstätten austenite (γ_w). For the solidified zone, with Ar + 2% N_2 (Figure 6c), elongated and thicker austenite grains are evident.

Figure 7 shows the cross-section profile of nitrogen amounts in mass%, for sheet welded with pure Ar. As reported in the literature, the loss of nitrogen in ZTA and SZ are unavoidable in GTAW welding using pure Ar as shielding gas[13,15,37]. Hosseini et al.[37] obtained a cross-section profile of nitrogen in superduplex stainless steel subjected to a GTAW arc by WDS analysis. The author still considers the amount of nitrogen in the solidified zone as virtually zero. As seen in Figure 7, a large number of point measurements of nitrogen within the ZTA and SZ are zero. The loss of nitrogen is accompanied by the reduction of the amount of austenitic phase leading to a lower corrosion resistance and loss of mechanical properties[10].

The Figure 7b, presents a slightly more expressive nitrogen amount content profile for samples welded with the gas mixture Ar + 2% N_2 as protection gas. However, the reduction of the amount of nitrogen is relative to the base metal, which is evident. Zhang et al.[15] assessed the content of nitrogen for each phase in the welding zone through quantitative element mapping using EPMA. As reported by Zhang, the 2% N_2 addition in the shielding gas also promoted the nitrogen solution in the austenite[15]. According to Lin et al.[31], experimental results show that the heat input increases with the increased welding voltage caused by the increased nitrogen content of the shielding gas. The authors also observed steeply decreases of the ferrite amount using nitrogen in shielding gas.

For the present work, it was also observed a higher concentration of nitrogen in allotriomorphic austenite (γ_A) grains than in austenite grains type Widmansttätten. This fact is reinforced by the low amount of nitrogen found for the measurements path as described in the nitrogen measurement profile. According to Eghlimi et al.[38], the lowest amount of Cr, Mo and N in the Widmansttätten austenite grains is due to their formation at low temperatures when most of the alloying elements have already been consumed by the allotriomorphic austenite grain boundaries.

The microhardness test was performed on the cross section of the welded samples. With the extracted data the microhardness maps were constructed and compared with the generated images from the microstructure of the welded region, as seen in Figure 8. The microhardness was measured in an area of 1.8 mm x 8 mm which surrounds the base metal with the position of the thermocouple, the ZAC and the SZ observed through the micrographs of the cross section from both samples.

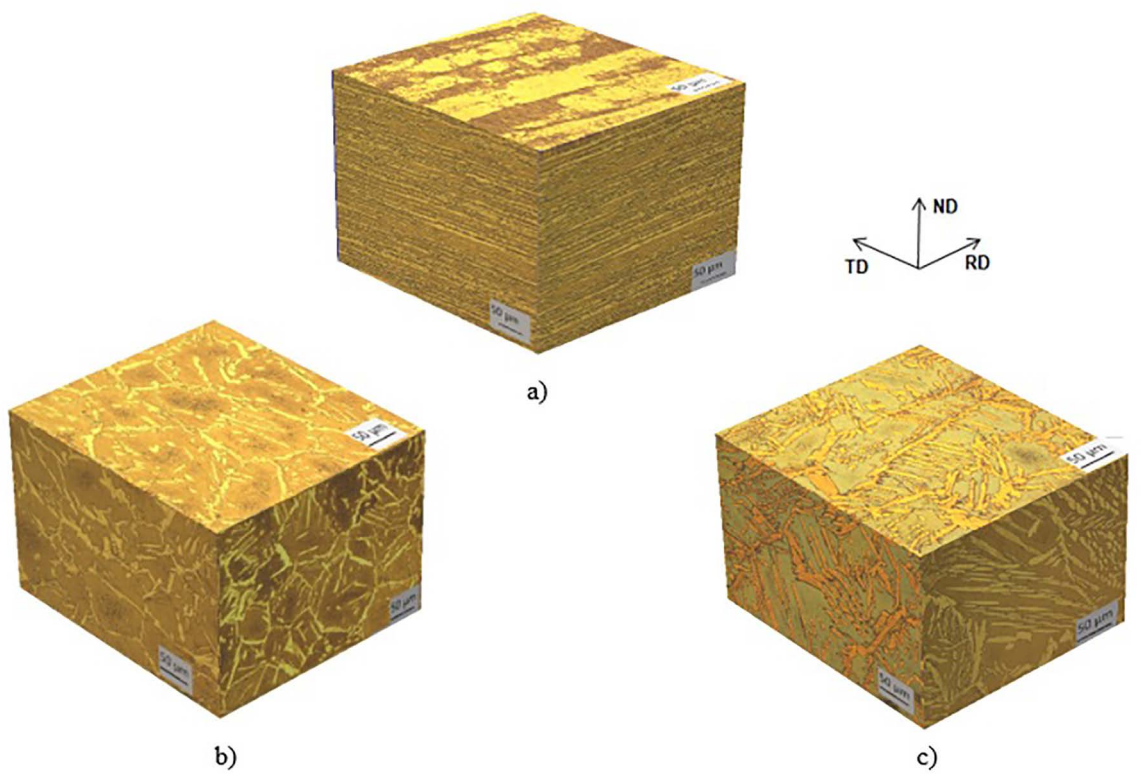

Figure 6. Three-dimensional microstructure of duplex stainless steel UNS S32304 welds in base metal and solidified zone of the GTAW welded joints using b) pure Ar and c) Ar+2%N_2 as shielding gas. The polishing samples were etched for 30 seconds in modified Behara I reagent, composed of 20 mL hydrochloric acid (HCl), 80 mL distilled water and 1 g potassium metabissulfide ($K_2S_2O_5$).

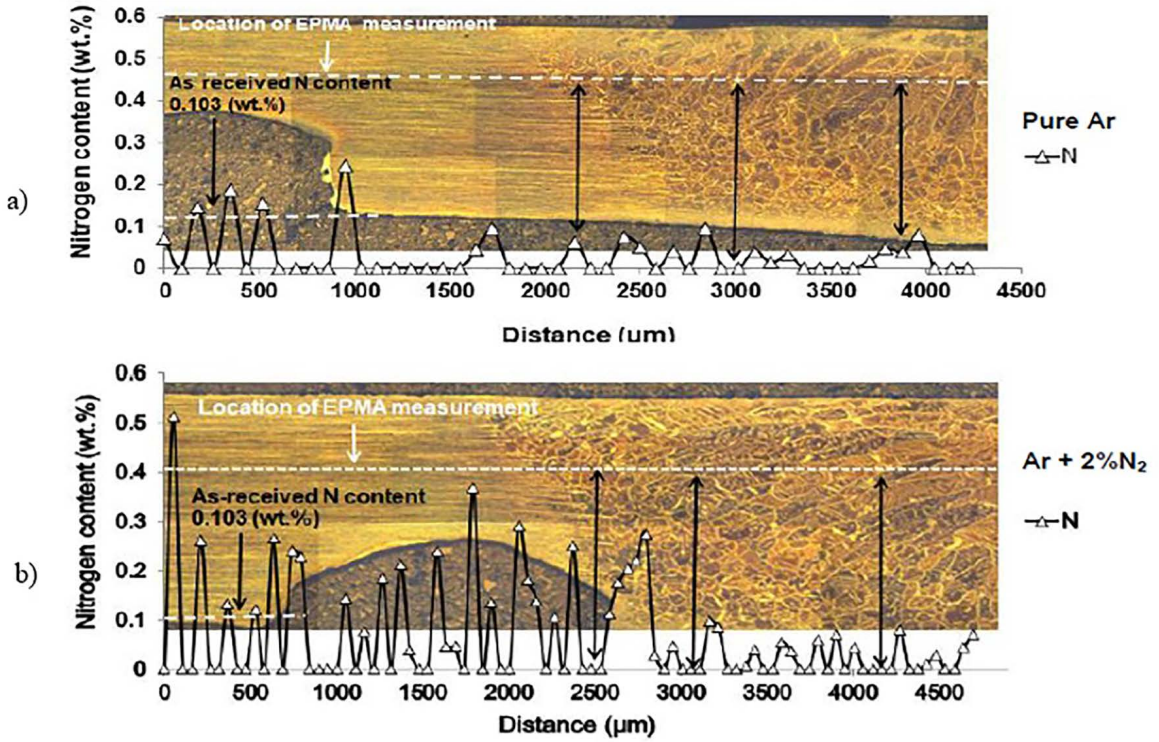

Figure 7. Nitrogen concentration as a function of transversal position measured by EPMA for both GTAW process with a) pure Ar and b) Ar+2%N_2 as shielding gas.

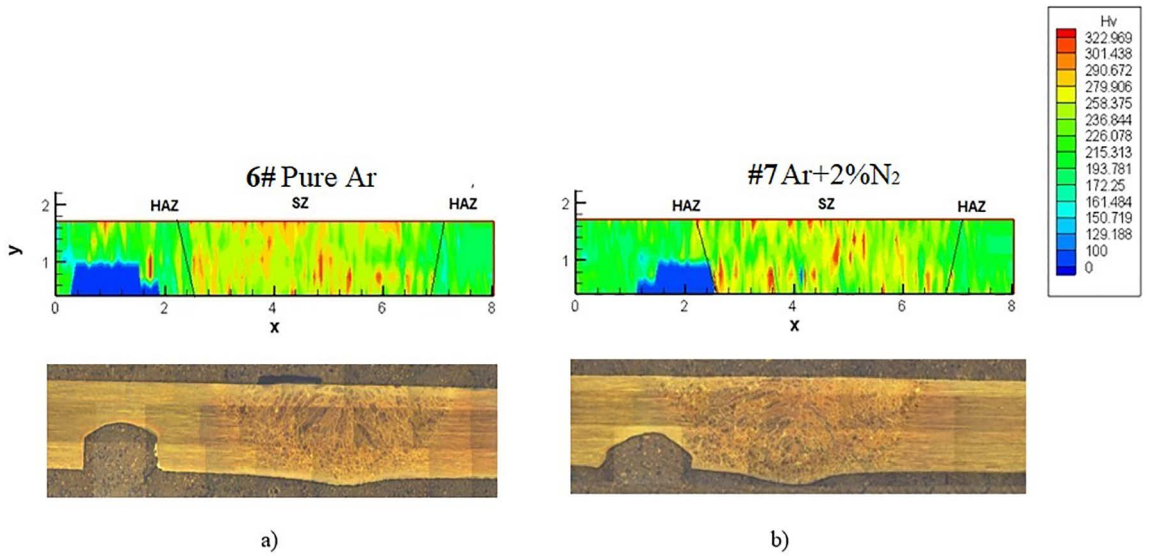

Figure 8. Microhardness maps on transversal direction of the GTAW welded joints using a) pure Ar and b) Ar+2%N_2 as shielding gas.

Observing the Figure 8, the base metal region highlighted in green on the microhardness map (approximately 220 $HV_{0.05}$) is in accordance with that informed by the steel supplier. The sample welded with pure Ar as protection gas, see Figure 8a, presented islands of hardness mainly at the center of the weld bead. The same phenomenon is observed for the sample welded with Ar + 2% N_2 (see Figure 8b), where the islands with high hardness are larger and more evident.

A large amount of allotriomorphic austenite (γ_A) of columnar ferrite grain contours is also observed in the micrographs, and especially in the equiaxial ones, with this region having higher hardness. The high amount of γ_A was favored by the high concentration of nickel and under the influence of N_2 in the shielding gas[39]. According to Ruiz et al.[39], the microhardness is higher in the austenite than in the ferrite and the nitrogen, as already discussed, contributes strongly to the austenite reforming.

4. Conclusion

Through the welding thermal cycles, it was possible to determine the temperatures of the duplex stainless steel in the melt pool and in the heat-affected zones. The higher peak temperature (947 °C) for the sample welded with addition of N_2 in the shielding gas did not directly imply on the increase of the cooling rate. The highest cooling rate was found for welding with pure Ar.

Based on results of the cooling rates and quantitative phase analysis, it was possible to conclude that the fast cooling of the welding zone is straightly related to the amount of austenitic phase. The amount of austenite decreased considerably for the sample welded using pure Ar. The intragranular austenite and grain edge for welded sample using pure Ar for three directions observed are smaller than ferrite for welding using the mixture Ar + 2% N_2 as the shielding gas, can suggest a direct relationship with the increase of microhardness in the solidified zone for this sample.

The addition of N_2 in the shielding gas increased the hardness of the solidified zone. By the nitrogen amount profile measurements in the cross section, it is shown that it is possible to achieve a good level of nitrogen in the microstructure with adequate shielding gas aiming the increase of austenite phase.

5. Acknowlodgments

The authors want to thank Erasmus Mundus (EBW+), CAPES and CNPq for the financial support.

6. References

1. Gunn NR, ed. Duplex stainless steels, microstructure, properties and applications. Cambridge, UK: Abington Publishing; 2003.
2. Alvarez-Armas I. Duplex stainless steels: brief history and some recent alloys. *Recent Patents on Mechanical Engineering*. 2008;1(1):51-57.
3. Messer B, Oprea V, Wright A. Duplex stainless steel welding: best practices. Stainless Steel World. 2007:53-63.
4. Pohl M, Storz O, Glogowski T. Effect of intermetallic precipitations on the properties of duplex stainless steel. *Materials Characterization*. 2007;58(1):65-71.
5. Bettahar K, Bouabdallah M, Badji R, Gaceb M, Kahloun C, Bacroix B. Microstructure and mechanical behavior in dissimilar 13Cr/2205 stainless steel welded pipes. *Materials & Design*. 2015;85:221-229.
6. Liou HY, Tsai WT, Pan YT, Hsieh RI. Effects of alloying elements on the mechanical properties and corrosion behaviors of 2205 duplex stainless steels. *Journal of Materials Engineering and Performance*. 2001;10(2):231-241.
7. Cárcel-Carrasco FJ, Pascual-Guillamón M, Pérez-Puig MA. Effects of x-rays radiation on AISI 304 stainless steel welding with AISI 316l filler material: a study of resistance and pitting corrosion behavior. *Metals*. 2016;6(5):102.
8. Fujii K, Fukuya K. Effects of radiation on spinodal decomposition of ferrite in duplex stainless steel. *Journal of Nuclear Materials*. 2013;440(1-3):612-616.
9. Betini EG, Gomes MP, Milagre MX, Machado CSC, dos Reis LAM, Mucsi CS, et al. Study on welding thermal cycle and residual stress of UNS s32304 duplex stainless steel selected as external shield for a transport packaging of Mo-99. *Brazilian Journal of Radiation Sciences*. 2019;7(2A):1-13.
10. Hosseini VA, Wessman S, Hurtig K, Karlsson L. Nitrogen loss and effects on microstructure in multipass TIG welding of a super duplex stainless steel. *Materials & Design*. 2016;98:88-97.
11. Valiente Bermejo MA, Karlsson L, Svensson LE, Hurtig K, Rasmuson H, Frodigh M, et al. Effect of shielding gas on welding performance and properties of duplex and superduplex stainless steel welds. *Welding in the World*. 2015;59(2):239-249.
12. Tseng KH, Chou CP. The effect of pulsed GTA welding on the residual stress of a stainless steel weldment. *Journal of Materials Processing Technology*. 2002;123(3):346-353.
13. Muthupandi V, Bala Srinivasan P, Seshadri SK, Sundaresan S. Effect of nitrogen addition on formation of secondary austenite in duplex stainless steel weld metals and resultant properties. *Science and Technology of Welding and Joining*. 2004;9(1):47-52.
14. Sales AM, Westin EM, Jarvis BL. Effect of nitrogen in shielding gas of keyhole GTAW on properties of duplex and superduplex welds. *Welding in the World*. 2017;61(6):1133-1140.
15. Zhang Z, Jing H, Xu L, Han Y, Zhao L, Zhou C. Effects of nitrogen in shielding gas on microstructure evolution and localized corrosion behavior of duplex stainless steel welding joint. *Applied Surface Science*. 2017;404:110-128.
16. Basyigit AB, Kurt A. The effects of nitrogen gas on microstructural and mechanical properties of TIG welded s32205 duplex stainless steel. *Metals*. 2018;8(4):226.
17. Moreno I, Almagro JF, Lovet X. Determination of nitrogen in duplex stainless steels by EPMA. *Microchimica Acta*. 2002;139(1-4):105-110.
18. Bobadilla M, Tschiptschin A. On the nitrogen diffusion in a duplex stainless steel. *Materials Research*. 2015;18(2):390-394.
19. Sieurin H, Sandström R. Austenite reformation in the heat-affected zone of duplex stainless steel 2205. Materials Science and Engineering: A. 2006;418(1-2):250-256.
20. Mohammed GR, Ishak M, Aqida SN, Abdulhadi HA. Effects of heat input on microstructure, corrosion and mechanical characteristics of welded austenitic and duplex stainless steels: a review. *Metals*. 2017;7(2):39.
21. Karlsson L, Arcini H. Low energy input welding of duplex stainless steels. *Welding in the World*. 2012;56(9-10):41-47.
22. Tan H, Wang Z, Jiang Y, Yang Y, Deng B, Song H, et al. Influence of welding thermal cycles on microstructure and pitting corrosion resistance of 2304 duplex stainless steels. *Corrosion Science*. 2012;55:368-377.
23. Xavier CR, Delgado Junior HG, de Castro JA. An experimental and numerical approach for the welding effects on the duplex stainless steel microstructure. *Materials Research*. 2015;18(3):489-502.

24. Chen L, Tan H, Wang Z, Li J, Jiang Y. Influence of cooling rate on microstructure evolution and pitting corrosion resistance in the simulated heat-affected zone of 2304 duplex stainless steels. *Corrosion Science*. 2012;58:168-174.

25. Westin EM. Microstructure and properties of welds in the lean duplex stainless steel LDX 2101(r). [Doctoral Thesis]. Stockholm: Royal Institute of Technology; 2010.

26. Tsuge H, Tarutani Y, Kudo T. The effect of nitrogen on the localized corrosion resistance of duplex stainless steel simulated weldments. *Corrosion*. 1988;44(5):305-314.

27. Bhatt RB, Kamat HS, Ghosal SK, De PK. Influence of nitrogen in the shielding gas on corrosion resistance of duplex stainless steel welds. *Journal of Materials Engineering Performance*. 1999;8(5):591-597.

28. Westin EM, Johansson MM, Pettersson RFA. Effect of nitrogen-containing shielding and backing gas on the pitting corrosion resistance of welded lean duplex stainless steel LDX 2101(r) (EN 1.4162, UNS S32101). *Welding in the World*. 2013;57(4):467-476.

29. ASTM International. ASTM E562-11 - Standard test method for determining volume fraction by systematic manual point count. West Conshohocken: ASTM International; 2011.

30. Garzón CM, Ramirez AJ. Growth kinetics of secondary austenite in the welding microstructure of a UNS S32304 duplex stainless steel. *Acta Materialia*. 2006;54(12):3321-3331.

31. Lin YC, Chen PY. Effect of nitrogen content and retained ferrite on the residual stress in austenitic stainless steel weldments. Materials Science and Engineering: A. 2001;307(1-2):165-171.

32. Tseng KH, Chou CP. Effect of nitrogen addition to shielding gas on residual stress of stainless steel weldments. *Science and Technology of Welding and Joining*. 2002;7(1):57-62.

33. Zucato I, Moreira MC, Machado IF, Lebrão SMG. Microstructural characterization and the effect of phase transformations on toughness of the UNS S31803 duplex stainless steel aged treated at 850 ºC. *Materials Research*. 2002;5(3):385-389.

34. Abas RHA, Taieh NK. Experimental study of the thermal diffusivity and heat capacity concerning some duplex stainless steel. *Al-Khwarizmi Engineering Journal*. 2015;11(2):51-61.

35. Tahaei A, Perez AFM, Merlin M, Reyes Valdes FA, Garagnani GL. Effect of the addition of nickel powder and post weld heat treatment on the metallurgical and mechanical properties of the welded UNS S32304 duplex stainless steel. *Soldagem & Inspeção*. 2016;21(2):197-208.

36. Badji R, Belkessa B, Maza H, Bouabdallah M, Bacroix B, Kahloun C. Effect of post weld heat treatment on microstructure and mechanical properties of welded 2205 duplex stainless steel. *Materials Science Forum*. 2004;467-470:217-222.

37. Hosseini VA, Karlsson L, Hurtig K, Choquet I, Engelberg D, Roy MJ, et al. A novel arc heat treatment technique for producing graded microstructures through controlled temperature gradients. *Materials & Design*. 2017;121:11-23.

38. Eghlimi A, Shamanian M, Raeissi K. Effect of current type on microstructure and corrosion resistance of super duplex stainless steel claddings produced by the gas tungsten arc welding process. *Surface and Coatings Technology*. 2014;244:45-51.

39. Ruiz A, Fuentes-Corona KJ, López VH, León CA. Microstructural and ultrasonic characterization of 2101 lean duplex stainless steel welded joint. *Applied Acoustics*. 2017;117(Pt A):12-19.